Acta Crystallographica Section A
Foundations of Crystallography
ISSN 0108-7673

Received 11 November 1999
Accepted 18 February 2000

Systematic intensity errors and model imperfection as the consequence of spectral truncation

Bart Rousseau, Stefan T. Maes and Albert T. H. Lenstra*

Department of Chemistry, University of Antwerp (UIA), Universiteitsplein 1, B-2610 Wilrijk, Belgium. Correspondence e-mail: lenstra@uia.ua.ac.be

The wavelength dispersion $\Delta\lambda/\lambda$ in a graphite (002) monochromated Mo $K\alpha$ beam was analyzed. A wavelength window was found with $0.68 < \lambda < 0.79$ Å, *i.e.* $\Delta\lambda/\lambda = 0.14$. The very large dispersion leads to systematic errors in $I_{\rm observed}(\mathbf{H})$ caused by scan-angle-induced spectral truncation. A limit on the scan angle during data collection is unavoidable, in order that an $\omega/2\theta$ measurement should not encompass neighboring reflections. The systematic intensity errors increase with the Bragg angle. Therefore they influence the refined X-ray structure by adding a truncational component to the temperature factor: B(X-ray) = B(true) + B(truncation). For an Mo tube at 50 kV, we find B(truncation) = 0.05 Å^2, whereas a value of 0.22 Å^2 applies to the same tube but operated at 25 kV. The values of B(truncation) are temperature independent. The model bias was verified *via* a series of experimental data collections on spherical crystals of nickel sulfate hexahydrate and ammonium hydrogen tartrate. Monochromatic reference structures were obtained *via* a synchrotron experiment and *via* a 'balanced' tube experiment.

1. Introduction

Tube spectra are polychromatic with characteristic emission lines superimposed on the white continuum. Several techniques such as β filters, balanced filters or crystalline monochromators exist to reduce the wavelength dispersion. However, a certain width $\Delta\lambda$ for the wavelength window is unavoidable.

While the phenomenon of dispersion is well known, its impact on X-ray structure determination is seldom realized. This paper sets out to measure and discuss some aspects of the problem. Here we confine ourselves to an experimental set-up that is representative of the usual situation in structure analysis. We work with a standard CAD4 diffractometer; the X-ray beam is generated *via* a sealed tube and it is monochromated *via* graphite (002).

Wavelength dispersion affects the shape of a Bragg reflection. Instead of a simple measurement at a reciprocal-lattice point, the observation gets more complicated, involving a rotation of the crystal, which is often combined with an angular shift in the detector position. The wavelength dispersion itself parallels an $\omega/2\theta$ scan mode. A finite wavelength dispersion in the incident X-ray beam is incorporated in the measuring strategy *via* the scan angle a, which is given by

$$a = \left(a_0 + \frac{\Delta\lambda}{\lambda}\frac{360}{2\pi}\tan(\theta)\right)^{\circ}.$$

Given this angular scan, each individual intensity is an integration over the whole spectral distribution characteristic of the primary X-ray beam. Studying the background on which Bragg intensities are superimposed, Maes *et al.* (1998) showed that wavelength dispersion could not be ignored as a potential source of systematic intensity errors.

When the scan angle a underestimates the real value for $\Delta\lambda/\lambda$, the observed intensities will systematically underestimate the real intensity due to spectral truncation errors. According to Denne (1977), this truncation leads to a structure model, in which the atomic displacement parameters are systematically too large. It is tempting to link this conclusion directly to the well documented inequality B(X-ray) > B(neutron) (see *e.g.* Craven & McMullan, 1979 and Blessing, 1995).

Denne's approach, which is based on the characteristic radiation only, has been criticized frequently (Ottersen *et al.*, 1982; Eisenstein, 1979) because it predicts incorrect values for the spectral truncation. The size of the latter has been estimated by Hirshfeld & Hope (1980), who found 40% errors on $|F|$ for high-order data. Destro & Marsh (1987, 1993) have reported intensity truncation errors of 15% for Mo data observed at Bragg angles of 20°.

Beam spectra are analyzed in §2. We find, for an incident X-ray beam with $\lambda = 0.71$ Å, monochromated *via* graphite (002), a wavelength dispersion of 0.14. This value does not depend on the tube's anode material because it is determined by the *Bremsstrahlung* alone. A discussion on the spectral

composition of the incident X-ray beam as a function of the monochromator, the selected wavelength *etc*. will be presented in a forthcoming paper.

In §3, we calculate the intensity errors due to truncation caused by a scan angle of $(1.3 + 0.4\tan\theta)^\circ$. At $\theta = 40^\circ$, an Mo tube operated at 50 kV produces *via* its spectral truncation an error of 10%. This error increases to 30% when $V_{\rm tube}$ is reduced from 50 to 25 kV. An increase in the temperature factor B is the logical response in the X-ray structure model to the spectral truncation error. For an Mo tube, we arrive at ΔB(truncation) of 0.05 and 0.22 Å^2 for 50 and 25 kV data, respectively. This behavior is verified in §4, in which a crystal of $NiSO_4{\cdot}6H_2O$ serves as an example. The experimental evidence supports the spectra-inferred B bias.

In §5, we present a 'monochromatic' structure determination. The monochromatic data set is obtained *via* a 'balanced-tube' experiment. It shows a shift in the atomic displacement parameters that matches the value of 0.05 Å^2 derived theoretically in §3.

Conclusions are drawn in §6.

2. The spectral distribution in the incident X-ray beam

We measured the wavelength dispersion in a graphite- (002) monochromated Mo beam using an Enraf–Nonius CAD4 diffractometer in combination with a sealed-tube X-ray generator. We used a fine-focus Mo tube and its take-off angle was set at 2.9° producing a focal spot of 0.4 × 0.4 mm. An Si (0,0,12) reflection, $\theta = 51.8^\circ$ for $\lambda = 0.71$ Å, served to analyze the spectral distribution characteristic for the incident X-ray beam. The size of the Si-analyzing crystal was 0.4 × 0.4 × 0.4 mm. Reflection profiles were measured with a 4 mm aperture slit in front of the detector. The crystal-to-detector distance is 208 mm. An $\omega/2\theta$ scan was used to record a reflection profile along the wavelength axis. In the end, we settled for a scan width of 21° in ω (or θ).

In a first series of repetitive profile scans, we used an incident X-ray beam generated by a tube setting of 50 kV and 20 mA. The averaged profile is depicted in Fig. 1. The error margin on *e.g.* the average background intensity of ~100 counts is practically 1%. The elastic Bragg intensity of the Si (0,0,12) is superimposed on this background. As can be seen in Fig. 1, the reflection starts at about $\theta = 48.8^\circ$ ($\lambda = 0.68$ Å) and it ends at about $\theta = 61^\circ$ ($\lambda = 0.79$ Å). The α_1/α_2 split is clearly visible and shows the expected 2:1 intensity ratio. The clear presence of a wavelength window with $0.68 < \lambda < 0.79$ Å indicates that the incident X-ray beam consists of two components, *viz*:

(i) the characteristic Mo $K\alpha$ radiation;

(ii) a white continuum contribution with wavelengths around 0.71 Å.

The presence of these two ingredients in the original X-ray beam is easily verified by a variation in $V_{\rm tube}$. Following Kramer's rule, I(*Bremsstrahlung*) varies linearly with $(V_{\rm tube} - V_\lambda)$, where $V_\lambda = 12\,400/\lambda$ (in Å). I(Mo $K\alpha$), however, changes exponentially *via* $(V_{\rm tube} - V_{\rm excitation})^n$. For Mo, $V_{\rm excitation} = 20$ kV. For $21 < V_{\rm tube} < 50$ kV, we observed a value of 1.6 for the exponent n.

The Si (0,0,12) profile observed with $V_{\rm tube} = 25$ kV is illustrated in Fig. 1. The error on the background intensity is ~4%. The ratio $I(\lambda|25\ {\rm kV})/I(\lambda|50\ {\rm kV})$ is theoretically 0.06 and 0.25 for the characteristic radiation and the *Bremsstrahlung*, respectively. As we can see in Fig. 1, these expected numbers match roughly with the observed ratios. This result shows that signal broadening due to thermal diffuse scattering is practically absent for Si (0,0,12) at θ(Mo $K\alpha$) = 51.8°. The signal width for the Mo Kα emission lines, characterized by an $I(25\ {\rm kV})/I(50\ {\rm kV})$ intensity ratio of 0.06 in the interval $0.707 < \lambda < 0.713$ Å, is limited to 0.8° in θ only. For the background intensity – incoherently scattered and thus not monochromatic – we find a ratio of 0.12 for $I(25\ {\rm kV})/I(50\ {\rm kV})$. This ratio is found at both sides of the coherent – and thus monochromatic – Bragg reflection, confirming our original estimate of 0.14 for the wavelength dispersion $\Delta\lambda/\lambda$.

At this point, we decided to inspect the wavelength selection by the graphite monochromator in more detail, which we achieved by avoiding the dominant Mo $K\alpha$ emission lines. We preserved the Mo geometry on the diffractometer but replaced the original Mo tube by a fine-focus Cu tube. Tube replacement

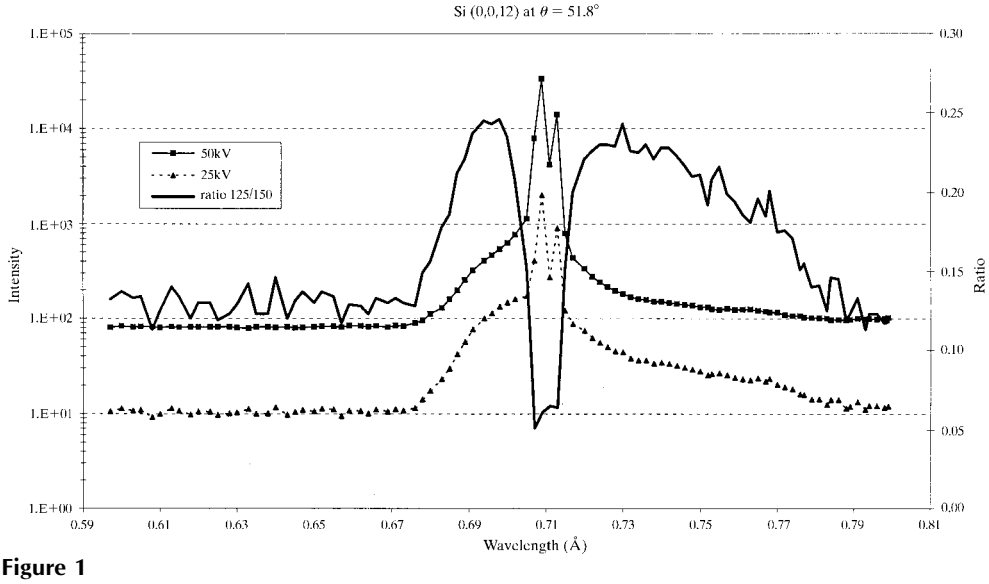

Figure 1
The reflection profile of Si (0,0,12) observed with a graphite (002) monochromated Mo $K\alpha$ beam; $41.3 < \theta < 62.3^\circ$. The intensity profiles are measured with a tube voltage of 50 kV (full line) and 25 kV (dashed line). The experimental ratio $I(25\ {\rm kV})/I(50\ {\rm kV})$ is indicated by the bold line.

causes in general a small shift in the position of the focal spot, forcing us to recalibrate the instrumental mean wavelength.

A redetermination of the Si unit cell pointed to an increase in λ from 0.71 to 0.715 Å. The Si (0,0,12) reflection profile observed with the Cu tube, operated at 50 kV and 20 mA, is shown in Fig. 2. λ_{start} has increased from ~0.68 (Fig. 1) to 0.685 Å in Fig. 2, in line with the unit-cell calibration. An independent verification of the assigned wavelength is possible by the introduction of a Y-absorption foil with $\lambda_{abs} = 0.728$ Å. We installed the Y foil just after the collimator, *i.e.* between the monochromator and the analyzing Si crystal. As we can see in Fig. 2, the Y-absorption edge causes an additional maximum in the (0,0,12) profile. The foil transmission changes from 40% ($\lambda < \lambda_{abs}$) to 80% ($\lambda > \lambda_{abs}$) at the absorption edge of 0.728 Å.

Using the white continuum of the Cu tube as light source, we find again a wavelength dispersion of 0.14 for the 'monochromated' X-ray beam.

3. Intensity errors caused by spectral truncation

The scan angle to be applied during data collection is given by $[a + (\Delta\lambda/\lambda)(360/2\pi)\tan\theta]^\circ$. This expression ensures that Bragg intensities are integrated over an angular range matching the wavelength window present in the incident X-ray beam. With a wavelength dispersion of 14%, one should measure reflections over an angular width of $(a + 8.0\tan\theta)^\circ$. This scan angle is large and it rapidly exceeds the separation between subsequent lattice points along, say, **c***. To measure individual intensities $I(00l)$, one is forced to use a much smaller scan angle. This leads automatically to the introduction of systematic intensity errors, in which $I_{observed} < I_{true}$ due to the deliberate limitation in the applied scan angle. The ratio $I_{observed}/I_{true}$ decreases with increasing Bragg angle because the discrepancy between the applied scan angle and the real value for $\Delta\lambda/\lambda$ gains importance.

We decided to calculate the intensity errors caused by spectral truncation introduced by a scan angle given by $(1.3 + 0.4\tan\theta)^\circ$. The calculations are based on the spectra shown in Figs. 1 and 2. The white continuum components in the tube spectra were described numerically *via* a polynomial expression:

$$\ln[I(\lambda)] = \sum_{i=0}^{5} b_i(\lambda - x)^i \quad \text{with } 0.68 < \lambda < 0.79\ \text{Å},$$

where $x = 0.71073$ Å and the coefficients b_i were obtained by least squares (25 kV: $b_i = 3.153$, -40.04, -3.748×10^3, 7.979×10^4, 9.145×10^5, -2.163×10^7; 50 kV: $b_i = 4.247$, -44.20, -2.504×10^3, 7.712×10^4, -6.264×10^5, 1.788×10^3).

For the characteristic Mo $K\alpha$ emission lines, we used a Lorentzian expression, *viz*

$$I(\lambda) = I(\alpha_1)\left[1 + 4\frac{(\lambda - \alpha_1)^2}{a_1^2}\right]^{-1} + I'(\alpha_2)\left[1 + 4\frac{(\lambda - \alpha_2)^2}{a_2^2}\right]^{-1},$$

in which α_1 and α_2 are the Mo $K\alpha$ wavelengths, $I(\alpha_1) = 2I'(\alpha_2)$, and the coefficients a_1 and a_2 were obtained by least squares. We found 0.00227 and 0.00089 Å for a_1 and a_2. Reflection profiles were calculated as a function of θ. These profiles were then used to arrive at the net intensity *via* the well known background–peak–background procedure. At $\theta = 0^\circ$, $I_{observed}$ equals I_{true} because there is no wavelength dispersion in the reflection profile at this angle. However, at $\theta = 40^\circ$, *i.e.* at $\sin\theta/\lambda = 0.9$ Å^{-1}, we find a significant overflow of the reflection signal into the local background. For the Mo tube at 50 kV, we find $I_{observed} = 0.9I_{true}$. When we reduce the tube tension to 25 kV, the truncation error increases to 30%, *i.e.* $I_{observed} = 0.7I_{true}$. The reduction in tube voltage reduces I(*Bremsstrahlung*) linearly, whereas I(Mo $K\alpha$) decreases exponentially. Consequently, the white continuum makes a relatively larger contribution to the total reflection intensity. At the same time, one should realize that the intensity truncation error is entirely determined by the *Bremsstrahlung* present in the 'monochromated' X-ray beam.

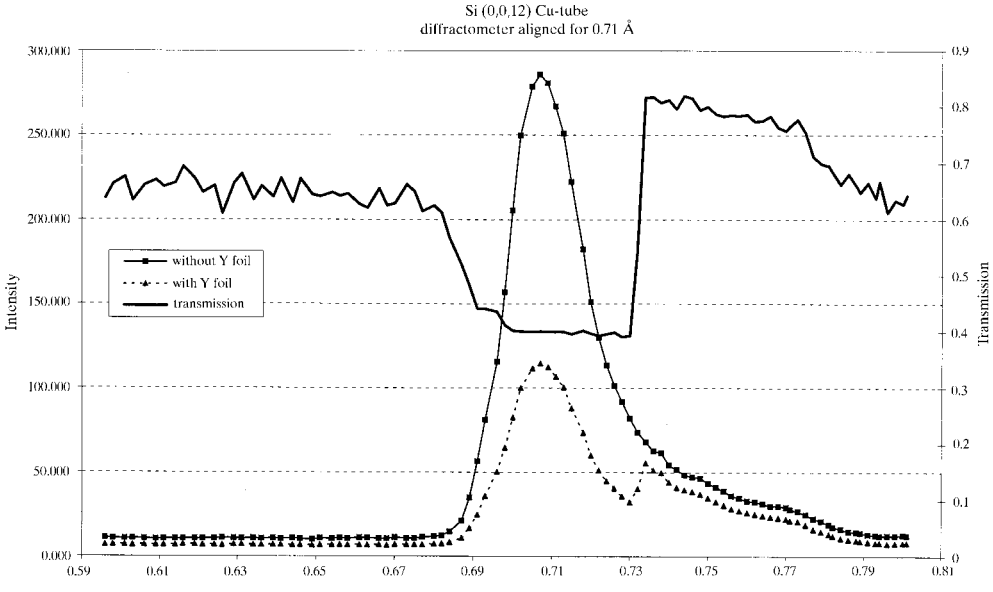

Figure 2
The Si (0,0,12) reflection observed with a graphite (002) monochromated Cu beam with λ centered at 0.71 Å. Cu tube operating at 50 kV. The full line corresponds to the original beam spectrum. The dashed line is the same profile but the beam impinging upon the crystal passed through a Y-absorption foil ($\lambda_{abs} = 0.728$ Å). The transmission through the foil is shown by the bold line.

Table 1
Summary of the least-squares results for $NiSO_4{\cdot}6H_2O$.

2995 data observed per structure ($0 < \sin\theta/\lambda < 0.9$ Å^{-1}); 80 variables refined with *Molen* package using $I > 3\sigma$.

	$I > 3\sigma$	R_u†	R_w‡	S	
300 K	2431	0.022	0.028	2.75	Mo; 50 kV
200 K	2268	0.024	0.029	1.25	
125 K	2119	0.023	0.035	1.97	
300 K	2028	0.029	0.028	2.16	Mo; 25 kV
200 K	1439	0.044	0.040	1.49	
125 K	1541	0.051	0.046	1.66	
300 K	759	0.044	0.040	1.49	Cu; 50 kV
200 K	1227	0.042	0.038	1.44	
125 K	1136	0.054	0.061	2.02	
300 K§	2649	0.047	0.116	1.12	Synchrotron; λ = 0.643 Å

† $R_u = \sum ||F_o| - F_c|| / \sum |F_o|$. ‡ $R_w = \left[\sum_w (|F_o| - |F_c|)^2 / \sum_w |F_o|^2\right]^{1/2}$. § Refinement using all intensities with the *SHELX* package.

The intensity truncation is depicted in Fig. 3. It shows all the characteristics of a normal Wilson plot. This suggests a direct link between the spectral truncation error and the temperature factor of the structure under investigation. For a non-vibrating crystal structure ($B = 0$ Å^2), we find in the reconstruction of the structure from the observed intensities a B value of 0.05 Å^2, when our rigid structure was measured using an Mo tube operating at 50 kV. At 25 kV, the same structure would have an instrumental B value of 0.22 Å^2. The results of the Cu-tube calculations suggest a bias in the temperature factor due to truncation errors by as much as 1 Å^2.

In this section, we linked the systematic intensity error directly to the ADP values in the structure looked at. This approach is in line with Eisenstein & Hirshfeld (1983). In our view, this is a logical step, because the temperature factor is the only parameter in a structure model that links the observed intensity with the Bragg angle.

4. Experimental verification

The spectral truncation error made during data collection causes systematic underestimation of the observed intensities and leads to an artificial increase in the atomic displacement parameters. We decided to assess the size of the ADP bias by looking at several data collections from the same crystal applying the measuring conditions used to analyze the spectral distribution in the monochromated X-ray beam (§2).

We collected three data sets on our CAD4 from the same spherical crystal of nickel sulfate hexahydrate.[1] The crystal radius was 0.25 mm. $NiSO_4{\cdot}6H_2O$ crystallizes in one of the enantiomorphic space groups $P4_12_12$ or $P4_32_12$ (Wyckoff, 1965). At room temperature, we found $a = 6.782\,(1)$ and $c = 18.274\,(3)$ Å. Reflections were observed in an $\omega/2\theta$ scan mode. The detector aperture was fixed at 3 mm at a crystal-to-detector distance of 208 mm. The scan angle was given by $(1.3 + 0.4\tan\theta)^\circ$, *i.e.* we assume a wavelength dispersion of 0.007 during data collection. The real value for $\Delta\lambda/\lambda$ is 0.14 (see §2). In all three data collections, (Mo|50 kV), (Mo|25 kV) and (Cu|50 kV), the reference wavelength was fixed at 0.71073 Å. This λ value defined the center of the reflection scan. 2995 reflections were measured in each data collection. We observed intensities with $0 < h < 12$, $0 < k < 12$, $0 < l < 33$ up to a maximum Bragg angle of 40° (0.9 Å^{-1}). A spherical absorption correction was applied ($\mu = 2.58$ mm^{-1}) but the transmissions varied only a little, from 0.42 up to 0.44.

Intensity control reflections were observed every hour. They did not show any significant variation in intensity. We calculated the experimental spread s^2 in order to determine the instrumental instability *via* $s^2 = \sigma^2 + (pI)^2$, where σ^2 is the counting statistical error. We found $p = 0.01$ and we added the corresponding instrumental variance to the counting errors. For the least-squares refinements, our reflections were weighted according to $1/s^2$. The results of the structure refinements are summarized in Tables 1 and 2. The positional coordinates in Table 2 are inferred from the data set collected with the Mo tube operated at 50 kV. The atomic positions in the three refined models were identical within 2 e.s.d.'s. This does not hold for the atomic displacement parameters. As we can see in Table 2, the averaged B_{eq} value shifts from 1.82 (Mo|50 kV) *via* 1.99 (Mo|25 kV) to 2.38 Å^2 (Cu|50 kV). The sequence corroborates the increasing B bias derived from the spectral distribution in §3. There we predicted a ΔB value of 0.17 Å^2 for B(Mo|25 kV) − B(Mo|50 kV). This value is practically equal to ΔB(equivalent) listed in Table 3. In the absence of characteristic Mo $K\alpha$ radiation, we expect a maximum B value. The difference B(Cu|50 kV) − B(Mo|50 kV) is about 0.5 Å^2 according to Table 3. So in the case of $NiSO_4{\cdot}6H_2O$ it is possible to increase B by as much as 1/3 of its initial value observed under routinely applied conditions (Mo|50 kV). Even that value is biased because in line with §3 we expect B(true) to be equal to B_{obs}(Mo|50 kV) − 0.05 Å^2.

A model refinement leads to B(true) if the relevant data set is not affected by scan truncation errors. A 'monochromatic' beam, *i.e.* a beam with a small value of $\Delta\lambda/\lambda$, is available at *e.g.* the synchrotron facilities at Brookhaven. According to Kvick (1988), the wavelength dispersion in the crystallographic beamline $\Delta\lambda/\lambda = 0.0002$. A measurement with $\lambda = 0.643$ Å was collected from the $NiSO_4{\cdot}6H_2O$ crystal. Intensities were measured using a CCD detector. As in our local observations, we refined the $NiSO_4$ structure on all intensities with $h, k, l > 0$ up to 0.9 Å^{-1}. The result is included in Table 2. We observe an instrumental bias of 0.09 Å^2 separating B(synchrotron) from the standard laboratory B(Mo|50 kV).

The intensity truncation errors present in a data set are dictated by the difference between the applied and the ideal scan angle. For a particular incident beam and a selected scan angle, the truncation error itself is fully determined by the

[1] Supplementary data for this paper are available from the IUCr electronic archives (Reference: SH0139). Services for accessing these data are described at the back of the journal.

Bragg angle θ. Consequently, the bias in the ADP values of a structure model should be temperature independent. In Table 3, we summarized the results of a change in temperature on the atomic ADP's. The intensity data were again measured on our CAD4 diffractometer. The crystal was cooled by an N_2 flow from an Enraf–Nonius FR 558-NH cryostat. As we can see from Table 3 and Table 2, the value for B(Mo|25 kV) − B(Mo|50 kV) ≅ 0.2 Å^2 is temperature independent. The same holds for B(Cu|50 kV) − B(Mo|50 kV) ≅ 0.5 Å^2.

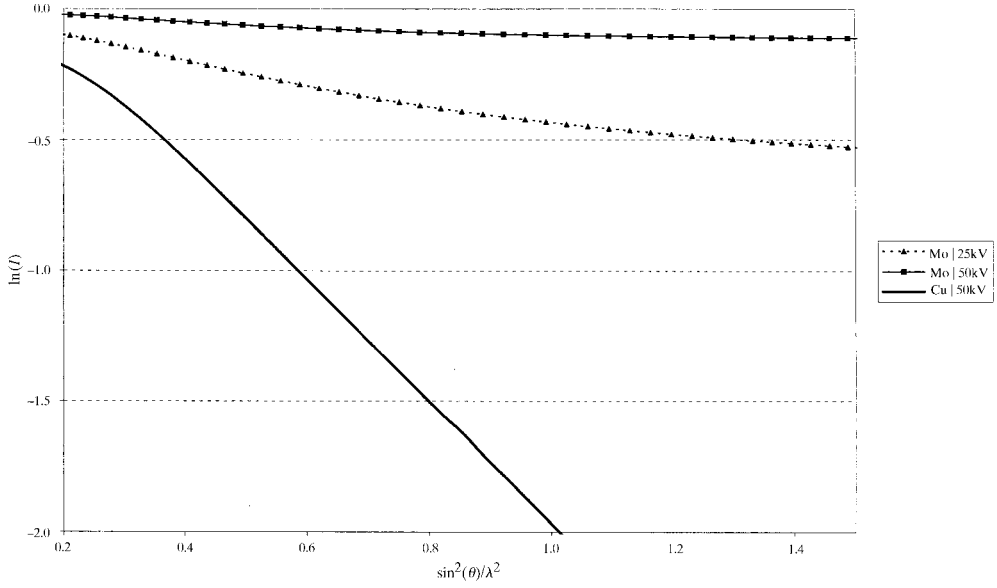

Figure 3
The intensity truncation error as a function of $(\sin\theta/\lambda)^2$ is illustrated *via* ln[I(observed)/I(true)]. In the absence of a characteristic emission line around $\lambda = 0.71$ Å, the white continuum of the Cu tube produces a maximum error (bold line). The minimum error is observed for an Mo tube operated at 50 kV (full line). At 25 kV, the Mo tube produces errors expressed by the dashed line.

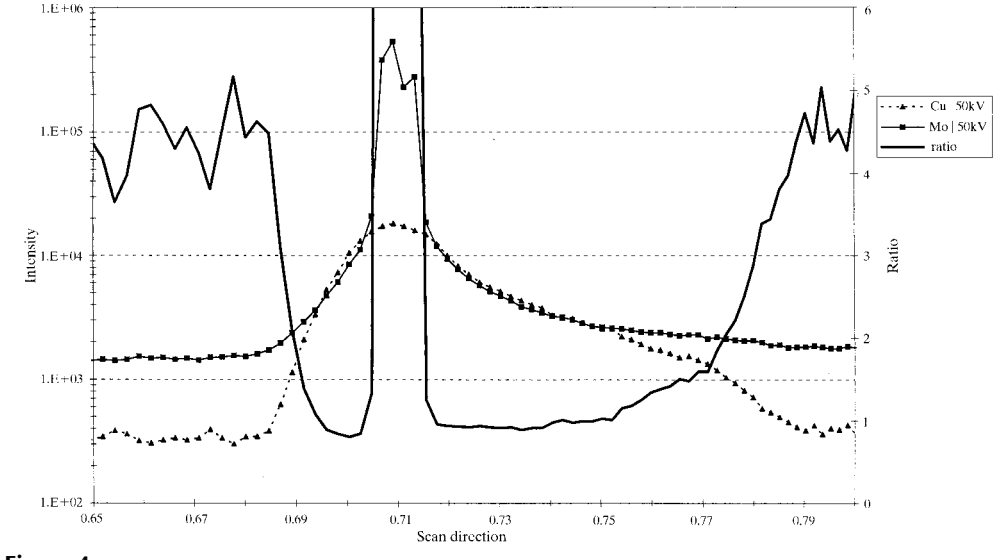

Figure 4
Si (0,0,12) reflection profile observed using graphite- (002) monochromated radiation. The coherently scattered signal originates from a fine-focus Mo tube (full line) and a Cu tube (dashed line). The intensity ratio (bold line) shows for the white continuum component that I(Mo) is practically equal to I(Cu).

5. A monochromatic data set *via* a balanced-tube experiment

The spectral composition of the X-ray beam impinging on the crystal to be analyzed is equipment related. On our CAD4/stationary-anode device, we found a wavelength dispersion of 0.14 as shown in the previous sections. For a Mach 3/rotating-anode combination, we observed $\Delta\lambda/\lambda = 0.09$ (see *e.g.* Fig. 5 in Lenstra *et al.*, 1998). Using graphite-monochromated Mo $K\alpha$ radiation, we noticed a significant decrease in the ADP values as the consequence of an increased tube voltage. This holds for any structure. In Table 4, we illustrate this point by showing the ADP values for ammonium hydrogen tartrate (van Bommel & Bijvoet, 1958) observed at 300, 200 and 125 K. All reflections of this orthorhombic structure were measured up to 30° in θ (Mo $K\alpha$) ($0 < h < 10$, $0 < k < 11$, $0 < l < 15$) in an $\omega/2\theta$ scan mode. We used a fixed aperture of 4.5 mm at a crystal-to-detector distance of 208 mm and a scan angle of $(0.8 + 1.0\tan\theta)°$. The difference between B(50 kV) and B(25 kV) is ~0.25 Å^2. This discrepancy is of the same size as the B difference found during the analysis of $NiSO_4{\cdot}6H_2O$ (0.22 Å^2).

When the tube's emission line is used in the scattering experiment, a high tube voltage will lead to a structure model in which the atomic displacement parameters are closer to the 'ideal' values, *viz* values typical for a monochromatic synchrotron experiment. It is possible to obtain the unbiased, or less biased, model with typical home-laboratory equipment *via* a double-tube experiment.

The first measurement was a standard one. Here it was the Mo data set of ammonium hydrogen tartrate observed with $V_{\rm tube} = 50$ kV. Every reflection in that data set is a sum of the characteristic radiation and a white continuum component. Without changing the diffrac-

Table 2
Positional and thermal parameters in $NiSO_4 \cdot 6H_2O$ at room temperature.

Unit-cell dimensions are $a = 6.782\,(1)$ and $c = 18.274\,(3)$ Å. The average value for B_{eq} is calculated from B(non-hydrogen) only. $B = 8\pi^2 U$.

				B_{eq} (non-H) (Å^2)			
	x	y	z	Mo; 50 kV λ = 0.71 Å	Mo; 25 kV λ = 0.71 Å	Cu; 50 kV λ = 0.71 Å	Synchrotron λ = 0.71 Å
Ni	0.71056 (2)	0.71056 (2)	0	1.120 (4)	1.285 (5)	1.57 (2)	1.020 (8)
S	0.20934 (4)	0.20934 (4)	0	1.300 (5)	1.466 (7)	1.88 (4)	1.215 (12)
O1	0.1209 (2)	0.1202 (2)	0.06583 (6)	2.46 (2)	2.64 (3)	2.90 (10)	2.42 (6)
O2	0.4236 (1)	0.1730 (2)	0.00038 (7)	2.18 (2)	2.36 (2)	2.68 (6)	2.11 (5)
O*W*1	0.6729 (2)	0.4533 (2)	0.05275 (7)	2.29 (2)	2.47 (3)	2.90 (10)	2.22 (5)
O*W*2	0.9704 (2)	0.7446 (1)	0.05613 (6)	1.76 (1)	1.89 (2)	2.40 (10)	1.64 (4)
O*W*3	0.5659 (2)	0.8562 (2)	0.08495 (5)	1.67 (1)	1.80 (2)	2.32 (9)	1.57 (4)
H1*W*1	0.596 (4)	0.373 (4)	0.042 (1)	3.5 (6)			
H2*W*1	0.732 (4)	0.429 (5)	0.082 (1)	4.3 (7)			
H1*W*2	1.048 (4)	0.663 (4)	0.049 (1)	2.4 (5)			
H2*W*2	1.028 (4)	0.848 (3)	0.061 (1)	2.8 (5)			
H1*W*3	0.511 (4)	0.944 (4)	0.071 (1)	3.3 (5)			
H2*W*3	0.500 (3)	0.786 (3)	0.113 (1)	2.2 (4)			
Average				1.83	1.99	2.38	1.74

Table 3
Thermal parameters of the non-hydrogen atoms in $NiSO_4 \cdot 6H_2O$.

At 200 K, the unit cell is given by $a = 6.799\,(1)$ and $c = 18.209\,(3)$ Å. This changes to $a = 6.775\,(1)$ and $c = 18.180\,(3)$ Å at 125 K. For the definition of B, see caption of Table 2.

	200 K			125 K		
	Mo; 50 kV	Mo; 25 kV	Cu; 50 kV	Mo; 50 kV	Mo; 25 kV	Cu; 50 kV
	λ = 0.71 Å	λ = 0.71 Å	λ = 0.71 Å	λ = 0.71 Å	λ = 0.71 Å	λ = 0.71 Å
Ni	0.712 (4)	0.887 (9)	1.20 (1)	0.486 (2)	0.65 (1)	0.88 (2)
S	0.841 (4)	1.036 (12)	1.40 (2)	0.553 (3)	0.80 (2)	1.13 (4)
O1	1.55 (2)	1.72 (5)	2.05 (5)	1.02 (1)	1.22 (5)	1.43 (9)
O2	1.34 (2)	1.53 (4)	1.85 (5)	0.88 (1)	1.10 (5)	1.37 (9)
O*W*1	1.61 (1)	1.84 (5)	2.08 (5)	1.12 (1)	1.32 (6)	1.6 (1)
O*W*2	1.13 (1)	1.30 (5)	1.62 (5)	0.82 (2)	1.03 (5)	1.16 (9)
O*W*3	1.11 (1)	1.30 (4)	1.63 (5)	0.78 (1)	0.98 (5)	1.4 (1)
Average	1.18	1.37	1.69	0.81	1.01	1.28

tometer alignment, we replaced the fine-focus Mo tube by a fine-focus Cu tube. A subsequent measurement of the ammonium hydrogen tartrate reflections resulted in a structure model in which the averaged value for B_{eq} is increased from its initial 1.97 Å^2 value to 2.59 Å^2. Every reflection in the Cu (λ = 0.71 Å) data set arises from the *Bremsstrahling* only. When we compare the Si (0,0,12) of the Mo measurement with the same profile for the Cu (λ = 0.71 Å) measurement, we see an almost equal intensity in the white continuum related parts in the reflection profiles. This is illustrated in Fig. 4. The intensity ratio in the nonmonochromatic background is 4.5, *i.e.* a weighted average between the intensities linked to the white continuum and the characteristic Mo radiation as observed in the coherent Bragg reflection. Therefore, a subtraction of the Cu measurement from the Mo measurement should produce a net intensity characteristic for Mo $K\alpha$ only. We used

$$I_{net} = I_{net}(\mathrm{Mo}) - I_{net}(\mathrm{Cu})$$

and

$$\sigma^2(I_{net}) = \sigma^2(I_{Mo}) + \sigma^2(I_{Cu}).$$

With this 'monochromatic' data set, we refined the structure of ammonium hydrogen tartrate. Relevant information is shown in Table 4. We notice a systematic decrease of 0.06 Å^2 in the B_{eq} values when we compare the monochromatic data set with the initial Mo $K\alpha$ measurement. This shift is of the same magnitude as observed in $NiSO_4 \cdot 6H_2O$, where we compared a synchrotron data set with the intensities of a stationary Mo anode.

6. Conclusions

The lack of monochromaticity in the graphite-monochromated Mo beam causes systematic intensity errors *via* scan-angle truncation. These intensity errors are dictated by the tube's *Bremsstrahlung*. Therefore, the final weight of the truncation error depends upon the tube voltage, which controls the intensity ratio

$$I(\text{characteristic emission})/I(\text{white continuum}).$$

As shown above, the intensity truncation error increases with the Bragg angle.

Table 4
Positional parameters of ammonium hydrogen tartrate at 300 K.

The thermal parameters of the non-H atoms are shown for 125, 200 and 300 K for data sets observed with an Mo tube operating at 50 and 25 kV. The room-temperature measurement was repeated with a Cu tube, *i.e.* with intensities dictated by *Bremsstrahlung* only. The 'monochromatic' set of B's was obtained using $[I(\text{Mo}|50\text{ kV}) - I(\text{Cu}|50\text{ kV})]$ as typical intensity of Mo $K\alpha$ alone.

				25 kV			50 kV			Cu	Mo $K\alpha$
	x	y	z	125 K	200 K	300 K	125 K	200 K	300 K	300 K	300 K
N1	0.1676 (2)	0.3110 (2)	0.4654 (1)	1.31 (4)	1.65 (5)	2.63 (7)	1.07 (3)	1.48 (3)	2.30 (3)	3.01 (8)	2.23 (3)
C1	0.9559 (2)	0.6387 (2)	0.7325 (1)	1.06 (5)	1.35 (5)	1.85 (7)	0.84 (3)	1.07 (3)	1.61 (3)	2.20 (8)	1.56 (3)
C2	0.7680 (3)	0.5736 (2)	0.7234 (1)	0.90 (4)	1.18 (5)	1.65 (6)	0.76 (3)	0.94 (3)	1.47 (3)	2.03 (8)	1.40 (3)
C3	0.6653 (2)	0.6839 (2)	0.6329 (1)	1.02 (4)	1.20 (5)	1.77 (6)	0.73 (3)	1.00 (3)	1.52 (3)	2.26 (8)	1.45 (3)
C4	0.4745 (2)	0.6222 (2)	0.6313 (1)	0.93 (4)	1.21 (5)	1.73 (6)	0.74 (3)	0.96 (3)	1.50 (3)	2.07 (8)	1.44 (3)
O1	1.0427 (1)	0.6192 (1)	0.63036 (9)	1.40 (3)	1.80 (4)	2.56 (5)	1.14 (2)	1.54 (3)	2.33 (3)	2.99 (6)	2.27 (3)
O2	1.0160 (1)	0.7004 (1)	0.82396 (9)	1.51 (4)	1.92 (4)	2.84 (5)	1.29 (3)	1.73 (3)	2.56 (3)	3.03 (6)	2.52 (3)
O3	0.6863 (1)	0.5797 (1)	0.83886 (9)	1.12 (3)	1.43 (4)	2.19 (5)	0.92 (2)	1.21 (3)	1.87 (2)	2.52 (6)	1.80 (2)
O4	0.6827 (1)	0.8613 (1)	0.65900 (9)	1.23 (3)	1.65 (4)	2.37 (5)	1.03 (2)	1.37 (3)	2.13 (2)	2.68 (6)	2.07 (3)
O5	0.4484 (1)	0.4641 (1)	0.61659 (9)	1.23 (3)	1.59 (4)	2.51 (5)	1.01 (2)	1.38 (3)	2.18 (3)	2.83 (6)	2.12 (3)
O6	0.3548 (1)	0.7325 (1)	0.64704 (9)	1.22 (3)	1.65 (4)	2.41 (5)	1.01 (2)	1.42 (3)	2.21 (3)	2.83 (6)	2.14 (3)
Average				1.18	1.51	2.23	0.96	1.28	1.97	2.59	1.91

Reflections at large reciprocal distances (Hirshfeld, 1976) should be almost free of bonding effects and thus they should properly reflect the vibrational smearing of the atomic core densities alone. This is clearly incorrect for X-ray structure models inferred from 'local' (nonsynchrotron) data sets. Our models contain an instrumental bias in the atomic displacement parameters. Algebraically, we have

$$B(\text{observed}) = B(\text{true}) + B(\text{truncation}).$$

The rigid-bond test looks at the relative vibrational motion of the bonded atoms A and C by comparing $z^2_{A,C}$ and $z^2_{C,A}$, *i.e.* the mean square atomic vibrations along the AC bond. This test will never identify B(truncation) because it influences A and C in the same way.

On our equipment, the intensity truncation errors are easily influenced by the choice of the scan angle and by the setting of the tube voltage. We find for an Mo tube that a reduction in the tube voltage from 50 to 25 kV increases the systematic error from 10 to 30% at $\theta = 40^\circ$. The magnitude of these errors matches the values reported by Destro & Marsh (1987, 1993). We find that B(Mo|50 kV) exceeds B(monochromatic/synchrotron or 'balanced' tube) by 0.08 Å^2. This is the minimum value for B(truncation) that we can obtain on our local equipment without interfering with the standard geometry of the diffractometer. Consequently, a CAD4-related structure model is characterized by

$$B(\text{X-ray}) = B(\text{true}) + B(\text{truncation}).$$

When we determine the same structure with a monochromatic neutron beam, we will find a mean square vibrational parameter equal to B(true). The lack of monochromaticity in the incident X-ray beam is in our opinion the main reason for the inequality B(X-ray) > B(neutron).

As illustrated in §3, it is not difficult to calculate B(truncation) from the observed beam spectrum using the selected scan angle. This suffices to show that an *a posteriori* intensity correction can be applied, in which I(observed) is upgraded into I(true). We get

$$I(\text{true}) = I(\text{observed}) \exp[2B(\text{truncation})s^2] \quad \text{with } s = \sin\theta/\lambda.$$

This calculation removes the artefacts caused by the white continuum component present in the incident X-ray beam. This correction is in practice the equivalent of the procedure proposed by Nelmes (1975) in which monochromatic intensities are calculated from the reflection profile generated by a β-filtered incident X-ray beam. When an analogous correction is applied to reflection profiles obtained with a graphite-monochromated X-ray beam, it is – surprisingly enough – regarded as a TDS correction (Blessing, 1987; Zavodnik *et al.*, 1999). In our opinion, the idea of a TDS correction is at best not yet relevant. We have two arguments, *viz*:

(i) TDS scattering is a pseudo-elastic phenomenon and thus wavelength shifts are too small to be observed. Our reflection profiles show clearly the Y-absorption edge at 0.728 Å. This illustrates the importance of the *Bremsstrahlung* in the incident beam.

(ii) In nickel sulfate as well as in ammonium hydrogen tartrate, we notice that B(truncation) is virtually temperature independent. If TDS were important, we would expect B(truncation) to decrease with decreasing temperature.

The authors are grateful to Dr Wu Guang for providing the synchrotron data. BR and STM acknowledge the Flemish governmental institution IWT for a predoctoral grant.

References

Blessing, R. H. (1987). *Crystallogr. Rev.* **1**, 3–58.
Blessing, R. H. (1995). *Acta Cryst.* B**51**, 816–823.
Bommel, A. J. van & Bijvoet, J. (1958). *Acta Cryst.* **11**, 61–70.
Craven, B. M. & McMullan, R. K. (1979). *Acta Cryst.* B**35**, 934–945.
Denne, W. A. (1977). *Acta Cryst.* A**33**, 438–440.
Destro, R. & Marsh, R. E. (1987). *Acta Cryst.* A**43**, 711–718.
Destro, R. & Marsh, R. E. (1993). *Acta Cryst.* A**49**, 183–190.
Eisenstein, M. (1979). *Acta Cryst.* B**35**, 2614–2625.

Eisenstein, M. & Hirshfeld, F. L. (1983). *Acta Cryst.* B**39**, 61–75.
Hirshfeld, F. L. (1976). *Acta Cryst.* A**32**, 239–244.
Hirshfeld, F. L. & Hope, H. (1980). *Acta Cryst.* B**36**, 406–415.
Kvick, Å. (1988). *Chemical Crystallography with Pulsed Neutrons and Synchotron X-rays, NATO ASI Series*, edited by M. A. Carrono & G. A. Jeffrey, p. 194. Dordrecht: Reidel.
Lenstra, A. T. H., Bracke, B., van Dijk, B., Maes, S., Vanhulle, C. & Desseyn, H. O. (1998). *Acta Cryst.* B**54**, 851–858.
Maes, S., Vanhulle, C. & Lenstra, A. T. H. (1998). *Acta Cryst.* A**54**, 399–410.
Nelmes, R. J. (1975). *Acta Cryst.* A**31**, 273–279.
Ottersen, T., Almlöf, J. & Carlé, J. (1982). *Acta Chem. Scand.* A**36**, 63–68.
Wyckoff, R. W. G. (1965). *Crystal Structures*, Vol III, 2nd ed, pp. 812–813. New York: John Wiley.
Zavodnik, V., Stash, A., Tsirelson, V., de Vries, R. & Feil, D. (1999). *Acta Cryst.* B**55**, 45–54.